Optical and Quantum Electronics 11 (1979) 525–539

Core fields in graded fibres with non-circular index contours

ADRIAN ANKIEWICZ
Department of Electronics, University of Southampton, Southampton, UK

Received 10 May 1979

Fields in the cores of graded non-circular optical fibres are analysed using a new method. It is shown that the scalar wave equation in elliptical co-ordinates can be separated for many realistic non-circular profiles, thus allowing calculation of fields by a double WKB method. The boundaries separating oscillatory and evanescent regions are found by simple analysis of algebraic equations. This method supports and further explains previous analysis which used geometric optics.

1. Introduction

Investigations of pulse propagation, measurements of refractive index profiles, and other experiments of optical fibre communications require a knowledge of light propagation in the fibres. The analysis used should yield results which are accurate, and yet simple enough to apply to practical situations. Some degree of ellipticity is often observed in graded-index fibres, so it is important to understand the effect of the deviation from circularity.

By introducing a new method, we show that for a wide range of non-circular profiles which are likely to occur, the mode fields in the core can be written in a relatively simple way. These fields provide an understanding of the ray path projections in non-circular fibres studied in [1], and may be used in further studies on propagation.

In Section 2 we provide the basic analysis and discuss the general patterns. In Section 3 we consider a simple case, the fields of the step-index fibre with an elliptical core–cladding interface. Section 4 gives limiting cases of the general theory. The modes of a parabolic-profile fibre which has circular refractive index contours are usually written in terms of functions based on either rectangular or circular polar co-ordinates. In Section 5, we derive a more general representation of these modes, and show that the tunnelling leaky modes are only marginally stable on the parabolic fibre, i.e. they can be removed by the introduction of an infinitesimal ellipticity. In Section 6 we consider how to apply this theory, once the refractive index profile is given; a typical class is analysed and results are compared with ray theory. Basic conclusions are given in Section 7.

2. Analysis of core mode fields

Our aim is to use elliptic cylinder (ξ, η) co-ordinate systems to represent modes in the cores of non-circular fibres. These co-ordinates are defined by:

$$\begin{aligned} x &= f\cosh\xi\cos\eta \\ y &= f\sinh\xi\sin\eta. \end{aligned} \tag{1}$$

Unlike rectangular (x, y) and polar (r, ψ) systems, there are infinitely many elliptical systems, as the focus parameter f can be varied from zero to infinity.

We consider fibres invariant in the z-direction, thus mode fields vary as $\exp(i\beta z)$. The exact fields satisfy Maxwell's equations, but in practice the refractive index changes very little in a distance of one wavelength, so the modes obtained by using the scalar wave approximation will be quite accurate [2].

0306–8919/79/060525–15$03.50/0

Each mode $E(x, y, z)$ satisfies the scalar wave equation,

$$[\nabla^2 + k^2 n^2(x, y)]E = 0 \tag{2}$$

where $n(x, y)$ is the refractive index and $k = 2\pi/\lambda$, with λ being the free-space wavelength.

Taking $E(x, y, z) = \Phi(x, y)\exp(i\beta z)$ we find,

$$[\nabla_t^2 + (k^2 n^2 - \beta^2)]\Phi = 0 \tag{3}$$

where

$$\nabla_t^2 \equiv \nabla^2 - \frac{\partial^2}{\partial z^2}.$$

Now in elliptical cylinder co-ordinates with focus parameter f

$$\nabla_t^2\Phi = \frac{1}{f^2(\sinh^2\xi + \sin^2\eta)}\left(\frac{\partial^2\Phi}{\partial\xi^2} + \frac{\partial^2\Phi}{\partial\eta^2}\right)$$

We set $\Phi = Q(\xi)S(\eta)$ and attempt to separate Equation 3:

$$\frac{1}{f^2(\sinh^2\xi + \sin^2\eta)}\left(\frac{1}{Q}\frac{d^2Q}{d\xi^2} + \frac{1}{S}\frac{d^2S}{d\eta^2}\right) + k^2n^2(\xi, \eta) - \beta^2 = 0. \tag{4}$$

This equation can be separated if we can find a value of f for which

$$n^2(\xi, \eta) = n_0^2 - \frac{g(\xi) + h(\eta)}{\sinh^2\xi + \sin^2\eta}. \tag{5}$$

Thus, given $n^2(x, y)$ we seek suitable $g(\xi)$, $h(\eta)$ and f. We shall see later that many realistic non-circular profiles can be written in this way. Then,

$$\frac{1}{Q}\frac{d^2Q}{d\xi^2} + \frac{1}{S}\frac{d^2S}{d\eta^2} + f^2(k^2n_0^2 - \beta^2)(\sinh^2\xi + \sin^2\eta) - k^2f^2[g(\xi) + h(\eta)] = 0.$$

By letting the separation constant be μ, we find

$$\frac{d^2Q}{d\xi^2} + k^2G(\xi)Q(\xi) = 0 \tag{6}$$

and

$$\frac{d^2S}{d\eta^2} + k^2H(\eta)S(\eta) = 0 \tag{7}$$

where

$$G(\xi) = f^2\left[\left(n_0^2 - \frac{\beta^2}{k^2}\right)\sinh^2\xi - g(\xi)\right] - \frac{\mu}{k^2} \tag{8}$$

and

$$H(\eta) = f^2\left[\left(n_0^2 - \frac{\beta^2}{k^2}\right)\sin^2\eta - h(\eta)\right] + \frac{\mu}{k^2}. \tag{9}$$

We obtain an approximate (WKB) solution to Equation 6 by taking

$$Q(\xi) = T(\xi)\,e^{ikW(\xi)}$$

and noting that k is large for optical frequencies:

$$Q(\xi) \sim |G(\xi)|^{-1/4}\exp\left\{\pm ik\int\sqrt{[G(\xi)]}\,d\xi\right\}.$$

Thus the field will be oscillatory when $G(\xi) > 0$, and evanescent when $G(\xi) < 0$. The boundaries

between the regions (caustics) are found simply from the zeros of $G(\xi)$. Thus,

$$Q(\xi) = \frac{A_1}{[G(\xi)]^{1/4}} \cos\left[k\int G^{1/2}\,d\xi + \phi_1\right];\ G(\xi)>0$$

$$= \frac{1}{[-G(\xi)]^{1/4}}\left(B_1 \exp\left[-k\int(-G)^{1/2}\,d\xi\right] + B_2 \exp\left[k\int(-G)^{1/2}\,d\xi\right]\right);\ G(\xi)<0 \quad (10)$$

where A_1, ϕ_1, B_1, B_2 are constants. The caustic position is the reference point in each integral. The nature of WKB type solutions of differential equations like Equations 6 and 7 has been studied in connection with quantum mechanics problems, and losses in optical waveguides [3–5]. It has been shown [6] that WKB solutions for mode fields are accurate everywhere, except close to the caustics. Clearly $Q(\xi) \to \infty$ when $G(\xi) \approx 0$, whereas physically there is a smooth transition from oscillatory to evanescent behaviour. Suppose ξ_1 is a zero of $G(\xi)$. By linearizing $G(\xi)$ in the neighbourhood of ξ_1, we see that the exact solution to Equation 6 in this region is a combination of Airy functions [7]. It shows the form of the change from oscillatory to evanescent behaviour near a caustic. We can find the constants in Equation 10 by comparing the WKB solutions on each side of the zero with the asymptotic forms of the exact solution.

Similarly,

$$S(\eta) = \frac{A_2}{[H(\eta)]^{1/4}} \cos\left[k\int H^{1/2}\,d\eta + \phi_2\right];\ H(\eta)>0$$

(oscillatory region)

$$= \frac{1}{[-H(\eta)]^{1/4}}\left(B_3 \exp\left[-k\int(-H)^{1/2}\,d\eta\right] + B_4 \exp\left[k\int(-H)^{1/2}\,d\eta\right]\right);\ H(\eta)<0 \quad (11)$$

(evanescent region)

where A_2, ϕ_2, B_3, B_4 are constants; they can be found by the method indicated for the constants in Equation 10.

Thus $\Phi = Q(\xi)S(\eta)$ is the product of two WKB type solutions. We get a propagating mode (oscillatory field) when $G(\xi)$ and $H(\eta)$ are both positive. For forms of $g(\xi)$ and $h(\eta)$ likely to occur, we can picture the following mode field patterns.

2.1. $\mu < 0$ (H type)

Here $G(0) > 0$, and $G(\xi)$ decreases to zero at $\xi = \xi_{tp}$. $H(0) < 0$, and for propagation we need $H(\pi/2) > 0$, i.e.

$$0 > \mu > -f^2(k^2 n_0^2 - \beta^2).$$

Then $H(\eta) > 0$ for $\eta_{min} < \eta < \pi/2$, where $H(\eta_{min}) = 0$. G and H are shown in Figs. 1a and b, respectively. Thus the mode is largely confined to the region

$$\left\{\begin{array}{l} 0 < \xi < \xi_{tp} \\ \eta_{min} < \eta < \pi/2 \end{array}\right\}$$

and the corresponding regions of the other quadrants. A typical pattern is shown in Fig. 1c. Modes like this will be called 'hyperbolic' or H type.

2.2. $\mu > 0$ (E type)

Here $G(0) < 0$, so there is an evanescent field near the centre. Generally, $G(\xi)$ will have two zeros in the core: ξ_{min} and ξ_{tp}. $H(0) > 0$ and $H(\eta)$ is generally positive for all η. Thus the field is oscillatory in the region $\xi_{min} < \xi < \xi_{tp}$. Figs. 2a and 2b show typical forms of G and H, and Fig. 2c shows a mode pattern of this type. This is an 'elliptic' or E type mode. Obviously, if f is outside the core, this type is not possible, as the curve $\xi = \xi_{tp}$ must be within the core, to ensure guided propagation.

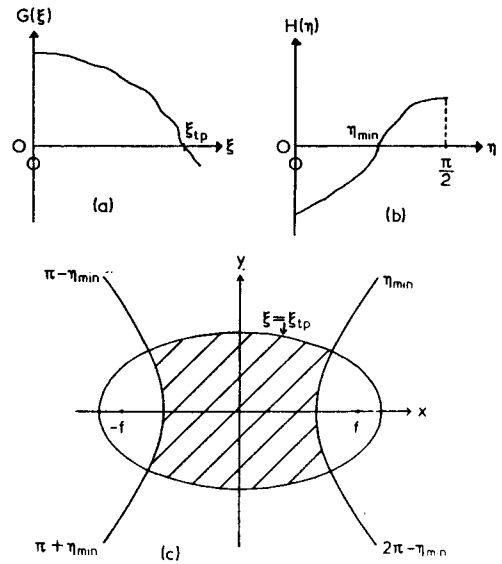

Figure 1 Forms of the functions $G(\xi)$ and $H(\eta)$, and the mode pattern for a 'hyperbolic' (H type) mode.

If we let the maximum refractive index be n_0, and let the index at the core–cladding interface be n_{cl}, then bound modes have $kn_{cl} < \beta < kn_0$, whereas leaky modes [5] have $\beta < kn_{cl}$.

The convenient feature of this method is that mode patterns can be found by simple analysis of algebraic equations. Ray path projections in graded non-circular fibres were studied in [1], and it was found that 'H' and 'E' types exist. Examples (found numerically) are shown in Figs. 3 and 4. By com-

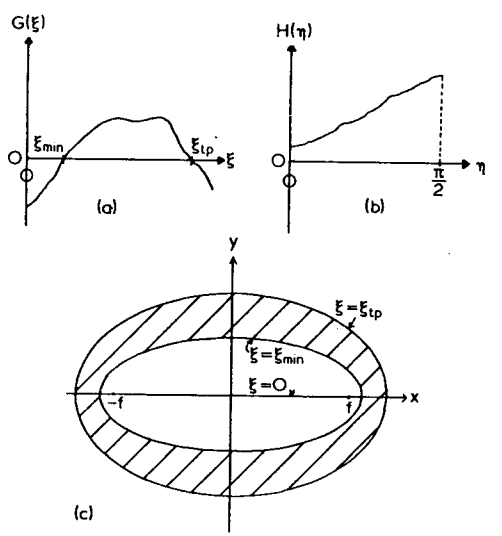

Figure 2 Forms of $G(\xi)$ and $H(\eta)$ and the mode pattern for an 'elliptic' (E type) mode.

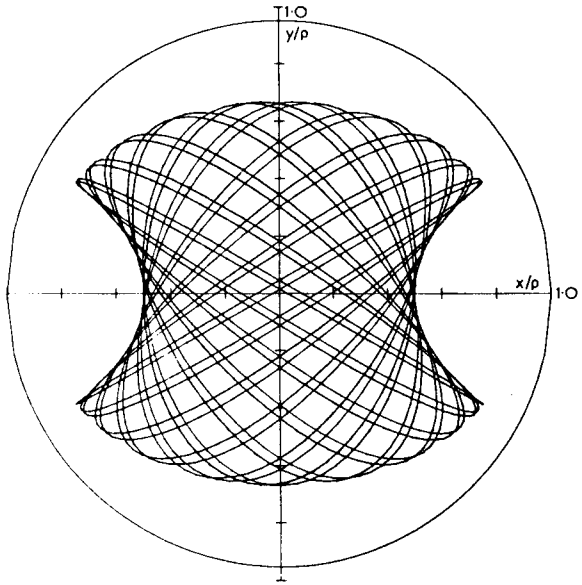

Figure 3 Example of 'hyperbolic' (H) type ray path projection on the cross-section of a non-circular graded-index fibre. The core–cladding interface is also shown; the eccentricity of the fibre is 5% in this case.

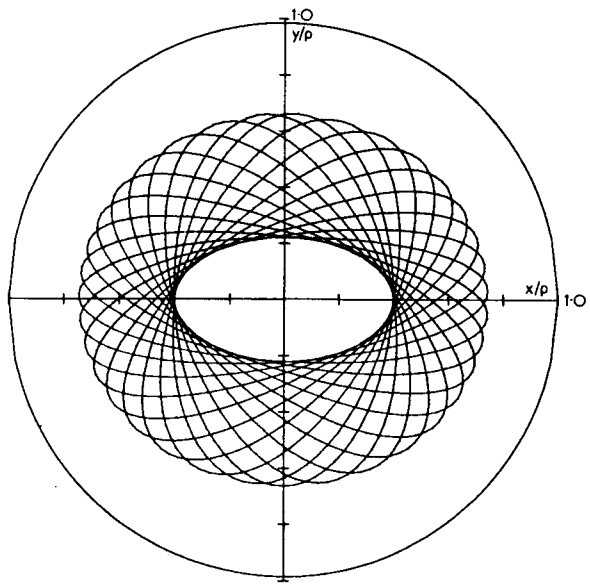

Figure 4 Example of 'elliptic' (E) type ray path projection. The eccentricity of the fibre is 1.5%.

paring Fig. 1c with Fig. 3, and Fig. 2c with Fig. 4, we see that the ray path projection on the cross-section forms the framework or 'skeleton' of the corresponding mode. The ray paths can be found numerically for any given index distribution.

3. Step-index fibre with elliptical boundary

As a first application, we consider a step-index ($n = n_0$) fibre with a core–cladding interface described by $\xi = \xi_b$, with focus f. This system has been considered previously [8, 9]. It is obtained simply by taking

$$h(\eta) = 0; \text{ for all } \eta$$

$$g(\xi) = 0; \ \xi < \xi_b.$$

For $\xi > \xi_b$, $g(\xi)$ is such that $G(\xi) < 0$. Then

$$G(\xi) = f^2(n_0^2 - \beta^2/k^2)\sinh^2\xi - \mu/k^2 \tag{12}$$

$$H(\eta) = f^2(n_0^2 - \beta^2/k^2)\sin^2\eta + \mu/k^2. \tag{13}$$

3.1. $\mu < 0$ (H type)

Here $G(\xi) > 0$ for $\xi < \xi_b$, and $G(\xi) < 0$ for $\xi > \xi_b$. We need $H(\pi/2) > 0$, so

$$0 > \mu > -f^2(k^2 n_0^2 - \beta^2).$$

Then $H(\eta) > 0$ for

$$\sin^2\eta > \frac{-\mu}{f^2(k^2 n_0^2 - \beta^2)} = \sin^2\eta_{\min}. \tag{14}$$

Thus for a given (β, μ) we get an H type mode (Fig. 1c), with the outer ellipse being $\xi = \xi_b$. The foci of the hyperbolae $\eta = \pm\eta_{\min}, \pi \pm \eta_{\min}$, are the foci of the core–cladding interface ellipse. This is sometimes called a 'bouncing ball' mode.

3.2. $\mu > 0$ (E type)

Now $G(0) < 0$, and G increases to zero at $\xi = \xi_{\min}$ where

$$\sinh^2\xi_{\min} = \frac{\mu}{f^2(k^2 n_0^2 - \beta^2)}. \tag{15}$$

Thus $G(\xi) > 0$ for $\xi_{\min} < \xi < \xi_b$, and $H(\eta) > 0$ for all η. These are elliptic type modes, as in Fig. 2c, with $\xi = \xi_b$ replacing ξ_{tp}. Hence $G(\xi)$ does not approach zero as $\xi \to \xi_b$. Such a mode is sometimes called a 'whispering gallery' mode.

The fields given by Equations 10 and 11 with G and H from Equations 12 and 13 correspond to the asymptotic forms of Mathieu functions, known to be the exact solutions of differential Equations 6 and 7 for this case. The features of these functions, as well as approximate eigenvalues, are given in [10].

4. Limiting cases

Optical fibres are usually analysed using either rectangular or circular polar co-ordinates. We now show that the results so obtained are the special cases $f \to \infty$ and $f \to 0$, respectively, of the theory presented in Section 2.

4.1. $f \to \infty$ (hence $\xi \to 0$ and $\eta \to \pi/2$)

In this limit $f\cos\eta \to x$ and $f\sinh \to y$. Thus

$$\begin{aligned} n^2 &\to n_0^2 - g(\xi) - h(\eta) \\ &= n_0^2 - g_1(y) - h_1(x) \end{aligned}$$

where $g_1(y) = g\,[\text{arcsinh}\,(y/f)]$

and $h_1(x) = h\,[\arccos(x/f)]$ (16)

From Equations 8 and 9,

$$G(\xi) \to -\mu/k^2 - f^2 g(\xi) = -\mu/k^2 - f^2 g_1(y) \tag{17}$$

$$H(\eta) \to f^2\left[n_0^2 - \frac{\beta^2}{k^2} - h(\eta)\right] + \frac{\mu}{k^2} = f^2\left[n_0^2 - \frac{\beta^2}{k^2} - h_1(x)\right] + \frac{\mu}{k^2}. \tag{18}$$

The oscillatory part is contained within a rectangle and the caustics x_m and y_m are found from the zeros of the above functions. Thus

$$g_1(y_m) = n_0^2 - \frac{\beta^2}{k^2} - h_1(x_m) = \frac{-\mu}{k^2 f^2}. \tag{19}$$

Now

$$n^2(x_m, y_m) = n_0^2 - g_1(y_m) - h_1(x_m) = \beta^2/k^2 > n_{cl}^2$$

as (x_m, y_m) must be in the core. Thus the modes are bound. The ray projections for such core profiles also fill rectangles. Now $f\,d\eta \to -\,dx$ and $f\,d\xi \to dy$

so

$$S \to H^{-1/4} \exp\left\{\pm ik \int \left[n_0^2 - \frac{\beta^2}{k^2} - h_1(x) + \frac{\mu}{k^2 f^2}\right]^{1/2} dx\right\} \tag{20}$$

and

$$Q \to G^{-1/4} \exp\left\{\pm ik \int \left[\frac{-\mu}{k^2 f^2} - g_1(y)\right]^{1/2} dy\right\}. \tag{21}$$

We now consider the analysis of such profiles in rectangular co-ordinates; this uses $\Phi = X(x)\,Y(y)$ in Equation 3:

$$\frac{1}{X}\frac{d^2X}{dx^2} + \frac{1}{Y}\frac{d^2Y}{dy^2} + k^2[n_0^2 - h_1(x) - g_1(y)] - \beta^2 = 0.$$

Taking δ as the separation constant, we obtain

$$\frac{d^2X}{dx^2} + k^2 H_1(x) X(x) = 0 \tag{22}$$

where

$$H_1(x) = n_0^2 - h_1(x) - (\beta^2 + \delta)/k^2$$

and

$$\frac{d^2Y}{dy^2} + k^2 G_1(y) Y(y) = 0 \tag{23}$$

where

$$G_1(y) = \delta/k^2 - g_1(y).$$

Thus

$$X \sim H_1^{-1/4} \exp\left(\pm ik \int H_1^{1/2}\, dx\right)$$

$$Y \sim G_1^{-1/4} \exp\left(\pm ik \int G_1^{1/2}\, dy\right).$$

Clearly $\delta = -\mu/f^2$, and X and Y are just the limiting forms of S and Q given in Equations 20 and 21.

4.2. $f \to 0$

Here $f \sinh \xi \to r$ and $\eta \to \psi$ where (r, ψ) are cylindrical polar co-ordinates. From Equation 5

$$n^2 \to n_0^2 - \frac{g(\xi)}{\sinh^2 \xi} = n^2(r). \tag{24}$$

Thus

$$G(\xi) = f^2[(n_0^2 - \beta^2/k^2)\sinh^2\xi - g(\xi)] - \mu/k^2 \to r^2 P(r)$$

where

$$P(r) = n^2(r) - (\mu/r^2 + \beta^2)/k^2. \tag{25}$$

Now

$$d\xi \to dr/r \quad \text{so} \quad \int G^{1/2}\, d\xi \to \int P^{1/2}\, dr$$

and

$$Q \to |r^2 P(r)|^{-1/4} \exp\left\{\pm ik \int \sqrt{[P(r)]}\, dr\right\} \tag{26}$$

$$H(\eta) \to \mu/k^2$$

so

$$S(\eta) \to \exp(i\mu^{1/2}\eta). \tag{27}$$

$$S(\eta + 2\pi) = S(\eta)$$

so $\mu^{1/2}$ must be an integer, say ν.

In these cases, where the refractive index is a function of r only, it is common to use $\Phi = R(r) \exp(i\nu\psi)$ in Equation 3, with ∇_t^2 in cylindrical polar co-ordinates. This gives

$$\frac{d^2R}{dr^2} + \frac{1}{r}\frac{dR}{dr} + k^2 P(r) R(r) = 0$$

where μ has been identified with ν^2 in $P(r)$. Taking $r = e^w$ gives

$$\frac{d^2R}{dw^2} + k^2 e^{2w} PR = 0.$$

So

$$R \sim |e^{2w}P|^{-1/4} \exp\left\{\pm ik \int (e^{2w}P)^{1/2}\, dw\right\} = |r^2 P(r)|^{-1/4} \exp\left\{\pm ik \int P^{1/2}\, dr\right\}$$

i.e. the same as the limit of Q, given by Equation 26.

5. Mode representations for parabolic profile with circular refractive index contours

The circularly symmetric fibre with a parabolic profile,

$$n^2(r) = n_0^2 - \gamma^2 (r/\rho)^2 = n_0^2[1 - 2\Delta(r/\rho)^2]; \quad r \leqslant \rho \tag{28}$$

$$\gamma^2 = 2\Delta n_0^2 = n_0^2 - n_{cl}^2$$

has received great attention in the literature, as it is close to the optimum shape for minimum pulse dispersion. By applying the theory of Section 2 to it, we can gain insight into the stability of tunnelling leaky modes with respect to slight non-circular perturbations. Clearly we can represent Equation 28 in the form of Equation 5 by taking

$$g(\xi) = f^2(\gamma^2/\rho^2)\sinh^2\xi\cosh^2\xi$$
$$h(\eta) = f^2(\gamma^2/\rho^2)\sin^2\eta\cos^2\eta.$$

The curious fact that Equation 28 can be represented in this way, no matter which value of f/ρ is chosen, will be discussed later. We have

$$G(\xi) = -f^4\frac{\gamma^2}{\rho^2}\sinh^4\xi + f^2\left(n_0^2 - \frac{\beta^2}{k^2} - \gamma^2\frac{f^2}{\rho^2}\right)\sinh^2\xi - \frac{\mu}{k^2} \tag{29}$$

$$H(\eta) = f^4\frac{\gamma^2}{\rho^2}\sin^4\eta + f^2\left(n_0^2 - \frac{\beta^2}{k^2} - \gamma^2\frac{f^2}{\rho^2}\right)\sin^2\eta + \frac{\mu}{k^2}. \tag{30}$$

For convenience let us define,

$$B = \frac{1}{\gamma^2}\left(n_0^2 - \frac{\beta^2}{k^2}\right). \tag{31}$$

Bound modes thus have $0 < B < 1$, whereas leaky modes have $B > 1$.

5.1. Mode classes

5.1.1. H type ($\mu < 0$)

These modes are of the form given in Section 2.1, and pictured in Fig. 1c, with

$$2\sinh^2\xi_{tp} = B\frac{\rho^2}{f^2} - 1 + \left[\left(B\frac{\rho^2}{f^2} - 1\right)^2 - \frac{4\mu\rho^2}{k^2f^4\gamma^2}\right]^{1/2}$$
$$2\sin^2\eta_{min} = 1 - B\frac{\rho^2}{f^2} + \left[\left(B\frac{\rho^2}{f^2} - 1\right)^2 - \frac{4\mu\rho^2}{k^2f^4\gamma^2}\right]^{1/2}. \tag{32}$$

If the distance from the centre to the corner point (ξ_{tp}, η_{min}) is r_{max}, then

$$r_{max}^2 = f^2(\cosh^2\xi_{tp} - \sin^2\eta_{min})$$
$$= B\rho^2$$

so $(r_{max}/\rho)^2 = B$. The point (ξ_{tp}, η_{min}) is in the core, so $r_{max} < \rho$ and $B < 1$. Thus these H modes can only be bound. In [1] it was shown that, for any $n(x, y)$, no H type rays are tunnelling.

If we consider the set of modes having the same β but different values of μ, then there are many ellipse–hyperbola regions, but all are contained within (and touch) the circle $r = r_{max}(\beta) = \rho B^{1/2}$. As a comparison, we see from geometric optics that the maximum distance, r_{tp}, from the centre for a meridional ray with normalized axial invariant B is also $\rho B^{1/2}$.

5.1.2 E type ($\mu > 0$)

As explained in Section 2.2, we must have $f < \rho$ for these modes. Such an E mode is contained within the region $\xi_{min} < \xi < \xi_{tp}$ (see Fig. 2c), where

$$\frac{2\sinh^2\xi_{tp}}{2\sinh^2\xi_{min}} = B\frac{\rho^2}{f^2} - 1 \pm \left[\left(B\frac{\rho^2}{f^2} - 1\right)^2 - \frac{4\mu\rho^2}{k^2f^4\gamma^2}\right]^{1/2}. \tag{33}$$

Of course $\xi_{min} > 0$, so $B > (f/\rho)^2$. This is also evident from geometric optics, as it corresponds to the fact that β/k must be less than the refractive index at the focus points:

$$(\beta/k)^2 < n_0^2 - \gamma^2(f/\rho)^2.$$

Here

$$\left(\frac{r_{max}}{\rho}\right)^2 = \frac{f^2}{\rho^2}\cosh^2\xi_{tp}$$
$$= \frac{1}{2}\left\{B + \frac{f^2}{\rho^2} + \left[\left(B - \frac{f^2}{\rho^2}\right)^2 - \frac{4\mu}{k^2\rho^2\gamma^2}\right]^{1/2}\right\}.$$

Hence

$$B - (f^2/\rho^2) > 2\mu^{1/2}/(k\rho\gamma). \tag{34}$$

Also r_{max}/ρ must be less than 1, so for $B > 1$, we have the condition

$$(1 - f^2/\rho^2)(B - 1) < \mu/(k\rho\gamma)^2. \tag{35}$$

From Equations 34 and 35 we see that the maximum possible value of B is

$$B_{max} = 2 - f^2/\rho^2 \tag{36}$$

indicating that $1 < B_{max} < 2$.

Thus infinitesimal non-circular perturbations to the parabolic profile can reduce B_{max} from 2 to 1, or any intermediate value. However, if the contours remain circular, but the power law profile exponent is changed slightly from 2, then the tunnelling leaky modes remain. This shows that the tunnelling leaky modes of the profile given by Equation 28 are only marginally stable. The effect on the corresponding ray domains (Fig. 2 of [11]) is shown in Fig. 5.

5.2. Limit forms for the modes

There are two sets of modes commonly used for the circularly symmetric fibre with a parabolic profile. One is based on rectangular co-ordinates, the other on polar co-ordinates. Using results from Section 4, we shall consider the limit forms of the fields as $f \to 0$ and $f \to \infty$, and their relation to the sets of modes mentioned.

5.2.1. $f/\rho \to \infty$

The fields $\Phi = QS$ are given by Equations 20 and 21, with $h_1(x) = (\gamma x/\rho)^2$ and $g_1(y) = (\gamma y/\rho)^2$ in Equations 17 and 18. The positions of the caustics, $x = x_m$ and $y = y_m$ are obtained from the zeros of G and H, i.e. from Equation 19:

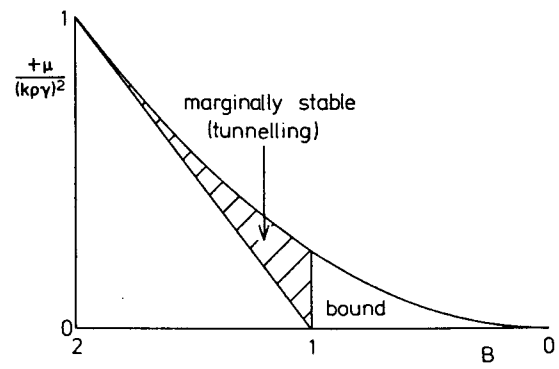

Figure 5 Effect of non-circular perturbation on ray domains for parabolic profile fibre with nominally circular contours. A slight deviation from circularity can reduce the maximum value of B from 2 to 1; hence the tunnelling leaky modes (and corresponding tunnelling rays) are only marginally stable.

$$\left(\frac{x_m}{\rho}\right)^2 = B + \frac{\mu}{k^2 f^2 \gamma^2}$$
$$\left(\frac{y_m}{\rho}\right)^2 = \frac{-\mu}{k^2 f^2 \gamma^2}. \tag{37}$$

These can also be derived from the limiting values in Equation 32. Thus

$$\left(\frac{x_m}{\rho}\right)^2 + \left(\frac{y_m}{\rho}\right)^2 = B$$

(cf. Equation 12 of [1]). The condition $H(\pi/2) > 0$ means

$$0 > \mu > -(kf\gamma)^2 B$$

so this limit produces rectangular mode patterns with

$$0 < x_m/\rho < 1; \quad 0 < y_m/\rho < 1.$$

The fields specified by Equations 20 and 21 are approximate solutions of differential Equations 22 and 23. In fact these equations can be solved exactly when h_1 and g_1 are as given above [2, 12]. Each mode field can be written as a product of two Hermite–Gaussian functions.

5.2.2. $f/\rho \to 0$

In this limit the fields $\Phi = QS$ are given by Equations 26 and 27. From the zeros of $P(r)$ (Equation 25) we see that the field is oscillatory in the annular region $r_{min} < r < r_{tp}$ where

$$\begin{matrix} r_{tp}^2 \\ r_{min}^2 \end{matrix} = \rho^2 \left\{ \frac{B}{2} \pm \left[\left(\frac{B}{2}\right)^2 - \left(\frac{\nu}{k\gamma\rho}\right)^2 \right]^{1/2} \right\} \tag{38}$$

The upper limit on ν is specified by

$$\frac{\nu}{k\gamma\rho} < \frac{B}{2}. \tag{39}$$

When $B > 1$, we also require

$$B - 1 < \left(\frac{\nu}{k\rho\gamma}\right)^2. \tag{40}$$

Clearly, $0 < B < 2$. (Bound modes have $0 < B < 1$). These are seen to be the limits $f/\rho \to 0$ of Equations 34–36. These modes can be written more precisely in terms of the Laguerre–Gaussian functions [13].

6. Mode fields in graded elliptical fibres

If we are given functions $g(\xi)$ and $h(\eta)$, then we can plot index contours on a graph with axes x/f and y/f. We now consider constraints on these functions and represent a class of non-circular profiles in terms of them.

As the focus points may be within the core, we need $n^2(\xi = 0, \eta = 0)$ finite. We are representing profiles in the form of Equation 5 and hence require $g(0) + h(0) = 0$; we take $g(0) = 0, h(0) = 0$. The profiles along the x- and y-axes are

$$\begin{aligned} n^2(0, \eta) &= n_0^2 - \frac{h(\eta)}{\sin^2\eta}; \quad |x| \leqslant f, \ y = 0 \\ n^2(\xi, 0) &= n_0^2 - \frac{g(\xi)}{\sinh^2\xi}; \quad |x| \geqslant f, \ y = 0 \\ n^2(\xi, \pi/2) &= n_0^2 - \frac{g(\xi)}{\cosh^2\xi}; \quad y\text{-axis.} \end{aligned} \tag{41}$$

Note that $n^2(0, \pi/2) = n_0^2$ (centre), so we get $h(\pi/2) = 0$. To ensure that the refractive index is continuous in the vicinity of the focus, we specify

$$\lim_{\xi \to 0} \frac{g(\xi)}{\sinh^2\xi} = \lim_{\eta \to 0} \frac{h(\eta)}{\sin^2\eta} = e^2 \text{ say}, \quad (\neq 0)$$

Thus for small ξ, η:

$$g(\xi) \approx e^2 \xi^2$$
$$h(\eta) \approx e^2 \eta^2.$$

For example, the above conditions are satisfied by

$$\begin{aligned} g(\xi) &= e^2 \sinh^2\xi \cosh^p\xi \\ h(\eta) &= e^2 \sin^2\eta \cos^p\eta; \quad p \geqslant 0 \end{aligned} \tag{42}$$

and we can choose f and p to represent various forms. In this case,

$$\begin{aligned} n^2(0, \eta) &= n_0^2 - e^2 \cos^p\eta \\ n^2(\xi, 0) &= n_0^2 - e^2 \cosh^p\xi \\ n^2(\xi, \pi/2) &= n_0^2 - e^2 \sinh^2\xi \cosh^{p-2}\xi. \end{aligned} \tag{43}$$

Taking $p = 2$ gives the circular parabolic profile discussed in Section 5.

As an example, we consider 'power-law' profiles of the form

$$n^2 = n_0^2 - \gamma^2 \left(\frac{x^2}{\rho^2} + \frac{b^2 y^2}{\rho^2}\right)^{q/2}; \quad x^2 + b^2 y^2 \leqslant \rho^2. \tag{44}$$

Again $\gamma^2 = n_0^2 - n_{cl}^2$ where n_{cl} is the index at the core–cladding interface.

In these profiles, the contours of constant index are concentric ellipses, and b is the ratio of major to minor axis length of any contour ellipse. This class is analysed using geometric optics in [1], and ray path projections are traced out. Although such profiles cannot be represented exactly in the form of Equation 5, we shall see that they can be closely approximated by using Equation 42, and choosing e, p and f suitably, thus allowing us to explain why the ray path projections in [1] (and Figs. 3 and 4 here) appear to be enclosed by roughly confocal ellipses and hyperbolae. For a given profile it was found that the positions of the foci varied slightly when the initial conditions were changed. We now see that this occurs because the representation in the form of Equation 5 is not exact. We shall also see the reason why E type modes are possible for some values of (b, q) and not others.

By comparing Equations 43 and 44 along the (positive) x-axis we require

$$\begin{aligned} \gamma^2 (x/\rho)^q &\approx e^2 \cos^p\eta; \quad x \leqslant f \\ \gamma^2 (x/\rho)^q &\approx e^2 \cosh^p\xi; \quad x \geqslant f. \end{aligned} \tag{45}$$

Now $x = f \cosh\xi$ for $x \geqslant f$, and $x = f \cos\eta$ for $x \leqslant f$, so we can get exact matching on the x-axis by taking

$$\begin{aligned} p &= q \\ \text{and} \qquad e^2 &= \gamma^2 (f/\rho)^q. \end{aligned} \tag{46}$$

On the y-axis we have $y = f \sinh\xi$, and so require

$$\left(\frac{by}{f}\right)^q \approx \frac{y^2}{f^2} \left(1 + \frac{y^2}{f^2}\right)^{(q-2)/2} \tag{47}$$

where p and e from Equation 46 have been used. The functions in Equation 47 differ only slightly for practical values of b and q (b close to 1, q close to 2). They are equal for $y = 0$; if $q > 2$, they have a

cross-over point at $y = y_1$ where

$$\frac{y_1}{f} = [b^{2q/(q-2)} - 1]^{-1/2}. \tag{48}$$

As we wish to match the functions for $0 < y < \rho/b$, it is clear that the cross-over point should be placed somewhere near the middle of this region. Numerical analysis shows that $y_1 = 0.6\,\rho/b$ is appropriate, and that the values all over the core are very close when the axes are matched in this way. This specifies the position of the focus (on the x-axis):

$$\frac{f}{\rho} \approx \frac{0.6}{b}[b^{2q/(q-2)} - 1]^{1/2}; \quad q > 2. \tag{49}$$

For $q < 2$, there is no cross-over, so the profiles cannot be matched as above. Instead the focus must be on the y-axis:

$$x = f \sinh \xi \sin \eta$$
$$y = f \cosh \xi \cos \eta.$$

We now see that the indices on the y-axis are exactly matched by taking

$$p = q \tag{50}$$

and

$$e^2 = \gamma^2 (bf/\rho)^q.$$

For the x-axis:

$$\left(\frac{x}{bf}\right)^q \approx \frac{x^2}{f^2}\left(1 + \frac{x^2}{f^2}\right)^{(q-2)/2}. \tag{51}$$

There is now a cross-over point at $x = x_1$ where

$$\frac{x_1}{f} = [b^{2q/(2-q)} - 1]^{-1/2}. \tag{52}$$

The region considered is $0 < x < \rho$, and now $x_1 = 0.6\,\rho$ gives a close approximation. Thus the focus is on the y-axis, and

$$\frac{f}{\rho} \approx 0.6[b^{2q/(2-q)} - 1]^{1/2}; \quad q < 2. \tag{53}$$

Again, agreement over the whole core is very close.

The positions of caustics can be found from the zeros of $G(\xi)$ and $H(\eta)$ in Equations 8 and 9, with $g(\xi)$ and $h(\eta)$ from Equation 42, where the appropriate values of e, p and f are used. However the general field patterns are immediately evident from a consideration of the focus position. If the focus is outside the core ($f \geq \rho/b$ for $q < 2, f > \rho$ for $q > 2$), then only the H type modes are possible (all are bound), whereas when the focus is inside the core, both H and E types are possible. If the focus is only just within the core, then there will be relatively few E modes. We see from Equations 49 and 53 that as $q \to 2, f/\rho \to \infty$, and so the mode fields become more rectangular as we approach this line from either side. As $b \to 1 (q \neq 2), f/\rho \to 0$ and the E mode fields become more circular. These regions are shown in Fig. 6, and we immediately have an explanation for the ray classes found numerically. The lines, in Fig. 5 of [1], separating the regions where tunnelling rays are possible from the region where only bound rays can exist, are superimposed (dashed) on Fig. 6; they are seen to be quite close to the mode demarcation lines.

This modal theory thus supports and further explains the geometric optics results. The reason why there is a region where only H type rays are possible is that, in this region, the effective focus for the profile is outside the core. In [1] the ray projections for $q < 2$ and $q > 2$ appear to differ by a rotation of 90°; we now see that this is because the focus is on the y-axis in one case, and on the x-axis in the other. For $b \approx 1$, and $q \approx 2$, we see from Equations 49 and 53 that the two demarcation lines can be

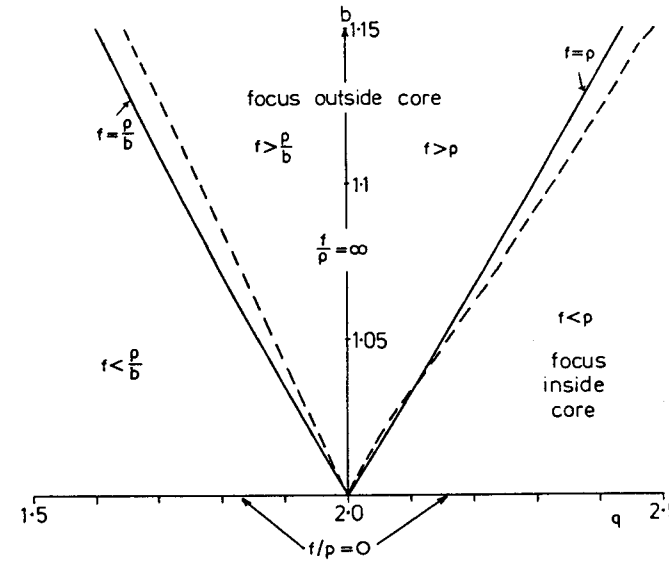

Figure 6 Focus positions for the class of fibres given by Equation 44. When the focus is outside the core, only H type modes are possible. The case $q = 2, b = 1$ (see Section 5) can be represented by any value of f/ρ, as all the lines intersect at this point. The dividing lines are obtained from Equations 49 and 53 for $q > 2$ and $q < 2$ respectively. When $q < 2$ the focus is on the y-axis, whereas it is on the x-axis when $q > 2$. The lines separating the region where only H type rays are possible from the region where both E and H types can exist [1] are shown dashed; they correspond closely to the lines where the focus is on the core–cladding interface.

approximated by the straight lines

$$b - 1 = 0.33\,|q - 2|. \tag{54}$$

7. Conclusion

We have shown that the core field pattern of a non-circular graded fibre can be found easily if it can be represented in the appropriate way. This rests on the separability of the scalar wave equation in elliptical co-ordinates for such profiles. The two mode types discussed here have corresponding ray classes in the geometric optics analysis. The oscillatory region is confined largely between two confocal ellipses in the E modes, whereas in H modes, it is bounded by a hyperbola and an ellipse. The particular shapes, and possible types depend critically on the position of the focus. When the focus is outside the core, only bound modes are possible. For the elliptical step-index fibre, the focus is in the core, so both E and H modes are always possible. The modes for the parabolic fibre with circular contours are usually based on analyses in polar or rectangular co-ordinates. We have seen that these are obtained as limits from our analysis by taking the focus approaching 0 or infinity respectively, but that any focus position, $0 < f < \infty$, can be used in this case. For this profile, the tunnelling leaky modes are only marginally stable with respect to non-circular perturbations.

Slight deviations from circularity can have a substantial effect on mode shapes, and on the proportion of the various types. Thus it would often not be satisfactory to use circular results as an approximation [14].

The theory presented in this paper may be used in future determinations of core refractive index profiles for non-circular fibres, and in other experiments where a knowledge of mode fields is required.

Acknowledgements

I thank M. J. Adams for discussions on this topic, and the CSIRO (Australia) for financial support.

References

1. A. ANKIEWICZ, *Opt. Quant. Elect.* **11** (1979) 197–203.
2. D. MARCUSE, 'Light transmission optics' (Van Nostrand Reinhold, New York, 1972) p. 267.
3. A. S. DAVYDOV, 'Quantum mechanics' 2nd Ed. (Pergamon Press, Oxford, 1976).
4. J. P. GORDON, *Bell Syst. Tech. J.* **46** (1966) 321–32.
5. R. OLSHANSKY, *Appl. Opt.* **15** (1976) 2773–7.
6. A. H. HARTOG and M. J. ADAMS, *Opt. Quant. Elect.* **9** (1977) 223–32.
7. J. D. LOVE and C. WINKLER, *J. Opt. Soc. Amer.* **67** (1977) 1627–33.
8. C. YEH, *J. Appl. Phys.* **33** (1962) 3235–43.
9. J. B. KELLER and S. I. RUBINOW, Ann. Phys. **9** (1960) 24–75.
10. P. M. MORSE and H. FESHBACH, 'Methods of theoretical physics', (McGraw-Hill, New York, 1953) Ch. 11.
11. A. ANKIEWICZ and C. PASK, *Opt. Quant. Elect.* **9** (1977) 87–109.
12. K. PETERMANN, *A. E. U.* **31** (1977) 201–04.
13. W. STREIFER and C. N. KURTZ, *J. Opt. Soc. Amer.* **57** (1967) 779–86.
14. J. J. RAMSKOV HANSEN, G. JACOBSEN and B. HALLBERG, *Opt. Commun.*, **26** (1978) 331–34.